Sea surface height and mixed layer depth responses to sea surface temperature in the northwestern Pacific subtropical front zone from spring to summer

Chunhua Qiu[1,4], Hiroshi Kawamura[2], Huabin Mao [3], Jiaxue Wu [1,*]

1. The Center for Coastal Ocean Science and Technology, School of Marine Sciences, Sun Yat-sen University, Guangzhou 510275, China
2. Center for Atmospheric and Oceanic Studies, Graduate school of Science, Tohoku University, Japan
3. State key Laboratory of Tropical Oceanography, South China Sea Institute of Oceanology, Chinese Academy Science
4. Guangdong Provincial Key Laboratory of Marine Resources and Coastal Engineering, , School of Marine Sciences, Sun Yat-sen University

Corresponding author:

Jiaxue Wu

The Center for Coastal Ocean Science and technology

School of Marine Sciences

Sun Yat-sen University

135 Xin Gang Xi Road

Guangzhou 510275, China

Phone: +86-20-84113678

Fax: +86-20-84113678

E-mail: wujiaxue@mail.sysu.edu.cn

Abstract:

We investigated the variation in the sea level anomaly(SLA) and mixed layer depth (MLD) during the weakening of SST front in the north western Pacific Ocean, based on weekly satellite-derived products and *in situ* observations. We separated the study area into cold, front, and warm zones, according to the frontal position. We examined the steric height component of SLA, using air-sea heat flux and *in situ* observations. Seasonal variation in SLA, and steric height displayed a similar pattern: a peak value (~15 cm) in July-August, and low value (~-15 cm) in February-March. The correlation between SLA and SST reached a value of 0.76 in the cold and front zones, but it only 0.38 in the warm zone, which possibly resulted from the presence of subtropical countercurrent. MLDs also differed among the three zones. MLDs decreased gradually in the front zone with increases in SST. A linear relationship ($y = -4.46x + 156.47$) between MLD and SST could be used to estimate the MLD in the subtropical front zone. The different patterns of variation among the zones indicates an increase in the rated of weakening of the SST front.

1. Introduction

The subtropical front is a major oceanic feature of the North Pacific, separating the warm saline North Pacific Central Waters in the south from the cool fresh waters to the north. The sea surface temperature (SST) front modulates atmospheric conditions, such as wind speed and direction (e.g., Xie, 2004; Small et al., 2008), temperature, turbulent fluxes (Friehe et al., 1991), and deep atmospheric responses (Kobashi et al., 2008). All of these variables change significantly from one side of the SST front to the other, with an increase (decrease) in wind speed as the wind blows from cold (warm) to warm (cold) water across the front (Friehe et al., 1991).

The subtropical SST front has been suggested to be accompanied with mixed layer depth (MLD) and sea surface height (SSH) variations (e.g., Uda and Hasunuma, 1969; White et al., 1978; Qiu and Lucas, 1996; Qiu, 2002; Kobashi et al., 2008; Kobashi and Xie, 2012; Kobashi and Kubokawa, 2012;). Qiu et al. (2014) quantitatively examined the mechanisms of subtropical SST front in April - September, and reported that the air-sea heat exchanges induced the disappearance of the subtropical SST front. They also found that the geostrophic advection calculated from the gradient of SSH, was quite small compared to the net heat flux. Although the magnitude of SSH gradient was small, the SSH in the study area (130-160°E, 20-32°N) showed relatively large meso-scale variability (Kobashi and Kawamura, 2001), but the variation in SSH in the SST front zone is still not well understood.

There was a nonlinear relationship between net heat flux and MLD when the SST front weakened (Qiu et al., 2014). The oceanic MLD is primarily determined by the action of turbulent mixing of the water mass due to wind stress and heat exchange at the air-sea interface (Kara et al., 2003). MLD is associated with SSH variation, because cooling of the sea surface induces convection, and then convection results in MLD deepening, and induces a decrease in SSH (e.g., Monterey and Levitus, 1997; de Boyer Montegut et al., 2004). Atmospheric conditions, waves and eddies also contribute to the SSH (Stammer,1997). In the present study, we examined the relationships among SST, SSH, and MLD.

We investigated changes in the upper-layer based on a 7-year record of weekly products of Advanced Microwave Scanning Radiometer - Earth Observing System (AMSR-E) SSTs, altimeter data, and *in situ* observations in the northwestern subtropical Pacific Ocean (Figure 1). We focused on the variation in SSH and MLD during the evolution of the SST front, and the relationships among SST, SSH and MLD. Data and methods are described in Section 2, the main results and discussions are presented in section 3, and a summary and conclusion are presented in Section 4.

2. Data and Methods

The AMSR-E on the Aqua satellite has provided global observations of SST since 2002. We used AMSR-E Level 2 data from January 1, 2003, to December 31, 2009. The original spatial resolution was around 10 km, and we interpolated the products into $0.125° \times 0.125°$ grids. Two snap images were used. Data processing followed Qiu and Kawamura (2012). AMSR-E has no data gaps and therefore the data are suitable for investigating seasonal variation in subtropicals (Hosoda, et al., 2010). The AMSR-E data are also of sufficient resolution to detect variation in the SST front.

Merged sea level anomaly (SLA) data were used. The data came from two satellite missions, TOPEX/Poseidon and ERS, followed by Jason-1 and Envisat. These datasets provide stable sampling temporally (AVISO, 2006). The mapped altimetry dataset includes one map every 7 days with a (1/3) °spatial resolution on a Mercator grid (Ducet et al., 2000).

Daily surface flux products for 2003-2009 were derived from the National Center for Environmental Prediction/National Center for Atmospheric Research (NCEP/NCAR) reanalysis project. The spatial resolution was $2.5° \times 2.5°$. We obtained the net heat flux Q by summing the sensible heat net flux, latent heat net flux, net longwave radiation, and net shortwave radiation.

To investigate the vertical structure of the upper layer, the Global Temperature and Salinity Profile Program (GTSPP) 'Best Copy' data from 2003-2009 were used. The data include the full-resolution data from XBTs or CTDs from the ships, Argo

profiling float data, or fully processed and quality-controlled data from the organizations that provided the real-time low-resolution data to the GTS (Sun et al., 2010). The temperature/salinity profile data were first interpolated onto a 1- m vertical resolution grid, and subsequently the density ρ and pressure P for each depth were calculated. The temperature at depth z is T_z , and the *in situ* surface temperature is $T_{0.}$

3. Results and Discussions

3.1 Seasonal variation in the subtropical SST front

Figure 2 shows the seasonal variation in the SST front. The frontal strength, based on the magnitude of SST gradient, is shown in Figure 2a. At 20 - 32 °N, the SST gradient showed significant seasonal variation, with a large gradient from October to the following June, and a small gradient from June to September. The SST front weakened from April to September, as reported by Qiu and Kawamura (2012).

The monthly mean frontal positions are shown in Figure 2b. In different locations, the frontal position had different variations. The frontal position showed significant seasonal variation in the western part (130 – 135 °E), was stable throughout the year in the central region (135 – 150 °E), and shifted seasonally in the eastern part (150 -160 °E). Subtropical waters are influenced by the path of Kuroshio Current, and in some years, the Kuroshio mean path entered the western and eastern parts of our study area (Figure 2 of Sugimoto and Hanawa, 2014). Therefore, the different patterns of seasonality of the frontal position may have been induced by movement of this current's path. The 7-year mean frontal position (thick black line) and standard deviation of the frontal position (grey area) are shown in Figure 2c. The mean SST front was located at around 22 - 28°N, with a shifting range of about ±2 °. Based on the frontal position, we separated the study area into cold, front and warm zones. The shaded band-like area was defined as the subtropical SST front area, the cold zone was located to the north of front, and the warm zone was to the south of the front.

The weakening of the SST front was due to the large increase in SST in the cold zone and minor SST increase in the warm zone (Qiu et al., 2014). Therefore, we investigated the SSH in the cold, front and warm zones separately to assess the influence of the ocean on the SST front.

3.2 Sea level variation

3.2.1 SSH Variation

SSH depends on several ocean processes, including heating and oceanic currents (Stammer, 1997), as shown below:

$$\eta = \eta_s + \frac{1}{g\rho_0} p_b \quad (1),$$

where η_s is the steric height,

We examined the steric height anomaly using two methods: *in situ* GTSPP observations and air-sea heat balance. The anomaly using GTSPP is expressed as:

$$\eta_s(x,y,t) = -\frac{1}{\rho_0}\int_{-H}^{0}[\rho(x,y,z,t) - \rho_m(x,y,z)]dz \quad (2),$$

where $\rho(x,y,z,t)$ is water density, $\rho_m(x,y,z)$ is time mean water density, and ρ_0 is a typical density. The depth H stands for the reference depth taken to be 1000 m.

The anomaly based on air-sea heat balance is:

$$\eta_s(x,y,t) = \frac{\alpha(x,y,t)Q'(x,y,t)}{\rho_0 c_p}\Delta t + \eta_s(x,y,t-1) \quad (3),$$

where time interval Δt was set as 7-day. $\eta_s(x,y,0)$ was given by the satellite SLA on January 1, 2003. The thermal expansion coefficient $\alpha(x,y,t)$ was evaluated from Table A3.1 of Gill (1982), using Levitus's (1982) mean mixed-layer temperatures. The effect of pressure on $\alpha(x,y,t)$ was neglected. c_p is the specific heat of seawater at a constant pressure.

The final term in Equation (1) represents the bottom pressure caused by the fluctuation of barotropic currents, and can be derived from $\eta_b = \eta - \eta_s$.

The variation in SLA, and steric height components calculated from the above two methods are shown in Figure 3. Both SLA and steric height anomaly displayed significant seasonal variation, with negative values in winter and peak values (>15 cm)

in mid-summer. The seasonal cycle in SLA was consistent with that of steric height. The amplitude of the steric height anomaly was much larger to the north than that to the south of the SST front. The steric height anomaly calculated from GTSPP data (Equation 2) was considered to represent the true oceanic conditions. That derived from air-sea heat flux roughly displayed the temporal variation in the true steric height. However, some mesostructures to the south of the SST front (within the black boxes of Figure 3a,c) were excluded, possibly due to the coarse resolution of the NCEP/NCAR net heat fluxes or the loss of freshwater flux.

3.2.2 SSH responses to SST

To elucidate the variation in SSH and SST, we used an empirical orthogonal function (EOF) analysis. The EOFs accounted for 26.3%, 15.4%, 4.5%, and 3.6% of the SLA variance for the first to fourth modes, respectively (Figure 4). Their contributions were relatively small compared to that obtained by Isoguchi et al. (1997), which is possibly due to the different study region and periods. The first EOF displayed a sharp height gradient, and its time series indicated that the SLA had significant seasonal variation. In summer, the SLA displayed a positive value in the cold zone, and a negative value in the warm zone. The second, third, and forth EOFs were dominated by multi-eddies, which were possibly influenced by oceanic currents.

The EOF analysis for SSTs is shown in Figure 5. The first mode of SSTs displayed a similar spatial pattern (high in the south, low in the north) to that of the SLA, indicating that the first EOF of SLA could explain the steric height component. The second to fourth EOFs of SST also preserved many meso-scale eddies, but their spatial scales were much larger than that of SLAs. One would expect the EOFs analysis using weekly data to provide the seasonal cycle as the principal component /first mode, and it is intuitive that the variabilities in SLA and SST follow a meridional gradient and their dominant component was seasonal.

To highlight the heating season, scatter plots of SLA and SST are shown for April - September in Figure 6. We matched the weekly SLA, *in situ* steric height and

AMSR-E SSTs in each grid of 0.125. Then we obtained the zonal mean datasets over the 7 year period. In total, 365 weeks were derived. The relationships between SST and SLA are shown in Figure 6(a-c). The correlations between SLA and SST were 0.76, 0.76, and 0.38 in cold, front, and warm zones, respectively. For steric height and SST (Figure 6(d-f)), their correlations were 0.86, 0.84, and 0.79, respectively. In each zone, both the SLA and steric height increased by around 20 cm, with some short-term oscillations, from April to September (colors indicate in different months). From April to September, the SLA sharply increased due strong heating in the cold zone, but it no evident variation in the warm zone. Finally, the SLA displayed a similar value ~8 cm, across the entire study area in September. The balance in SLA across the cold and warm zones occurred in reaction to the weakening of the SST front.

We further examined the relationships between SLA and SST after removing the seasonal cycle, using a high-pass filter, and called the resulting values HP-SLA and HP-SST. They are shown in Figure 6 g-i. In the cold zone, HP-SLA and HP-SST displayed a weak linear relationship with a correlation of 0.4. In the front zone, the variation in HP-SSH was smaller than that in the cold and warm zones, but the variation in HP-SST was larger. In the warm zone, the relationship between HP-SLA and HP-SST was opposite to that in the front zone, indicating that the disturbances in SLA did not result from those in SST. The warm zone located in the area of subtropical countercurrent field reported by Kobashi and Kawamura (2001) contained three branches of geostrophic current. These suggests the possible significant influence of oceanic currents on SLA in the warm zone. In the cold and front zones, SLA cycles were dominated by steric height, which was induced by air-sea heat balances. But in the warm zone, SLA cycles were not related to the steric height anomaly, and were possibly induced by oceanic currents. A strong subtropical countercurrent occupied the warm zone (Kobashi and Kawamura, 2001; Qiu and Kawamura, 2012), which further suggests that variation in SLA is induce by the oceanic current in the warm zones.

3.3 Mixed layer depth responses

When examining the disappearance of the SST front, it is important to include MLD in the equation $\partial SST/\partial t \propto -Q/h$, where Q is the net heat flux anomaly, and h is the MLD. Qiu et al. (2014) suggested that the nonlinear relationship between net heat flux and MLD contributes significantly to the mechanisms involved in the weakening of the SST front.

To examine how the MLD responds to the SST front, we matched daily AMSR-E products with the ship-measured points. The match spatial window was 0.125°, and the temporal window was within 12 hours. Totally, 811 points were derived. Kara et al. (2003) compared several definition methods with the isotherm layer depth, and suggested that the temperature difference (0.6℃, calculated as $T_0 - T_z$) was suitable in the subtropical zone, where T_0 is the GTSPP SST, and T_z the temperature at depth z. Therefore, in the present study, we defined the MLD as the depth where T_0 - T_z = 0.6 ℃.

Monthly temperature profiles in the cold, front, and warm zones are shown in Figure 7a-c. Gray double-headed arrows show the range of SST, and black arrows indicate the range of MLD. The ranges of SST and MLD were larger in the cold zone than in the front and warm zones.

Scatter plots of SST and MLD are shown in Figure 8 a,b. As expected, the MLD decreased with increasing SST . The relationships between SST and MLD differed among the three regions. MLD was inversely proportional to SST, with values ranging from 10 m to 250 m in the cold zone; an irregular relationship between MLD and SST emerged in the warm zone; and a linear relationship was found in the front zone. The correlations between SST and MLD were -0.70, -0.34, and -0.68 in the cold, warm, and front zones, respectively. In the front zone, their linear relationship suited the function: y = -4.46x + 156.47, where y is MLD, and x is SST. Note that some singular points (within the red circle), were located outside the range covered by standard deviations of y - (-4.46x + 156.47)). When we investigated the singular points in Figure 8c, the singular points remained at the edge of a warm filament. This indicates

that the noise results from the match window, and that the linear relationship between MLD and SST was realistic.

The sharp decrease in MLD in the cold zone increased the rate of weakening of the SST front. The ocean gained heat from atmosphere, and then trapped this heat within the mixed layer, although a minor amount of heat was entrained into the layer below the mixed layer. The decrease in MLD could lead to heat being aggregated according to height, increasing the rate of temperature increase in the cold zone. A sharp increase in SST in the cold zone and a minor increase in the warm zone resulted in a weakening of the SST front in mid-summer. Therefore, the evolution of MLD increased the rate of weakening of the SST front in April-September.

4 Summary and concluding marks

We investigated the variation in SSH and MLD and their relationships with the SST front in the North Pacific subtropical area, using satellite altimeter SSH, AMSR-E SST, and *in situ* GTSPP data.

We separated the study area into cold, front, and warm zones. The strong seasonal cycles in SSH were dominated by steric height in the cold and front zones. A weak seasonal cycle in SSH appeared in the warm zone. During the period of SST front weakening, the correlation between SLA and SST was 0.76, 0.76, and 0.38 in the cold, front and warm zones, respectively. After removing the seasonal cycle, the amplitudes of SSH were small in the cold and front zones, but large in the warm zone. The large magnitude in the warm zone may possibly be explained by the subtropical countercurrent. The SSH achieved a balance between the cold and warm zones in mid-summer, which weakened the subtropical countercurrent.

MLD decreased with increasing SST, which appeared as a reverse proportional function in the cold zone and a linear relationship ($y = -4.46x + 156.47$) in the front zone. This relationship suggests the feasibility of retrieving MLD from satellite-derived SST products. The different patterns of variation in MLD among different zones possibly increase the rate of the weakening of the SST front.

Acknowledgement

This study was jointly supported by National Basic Research Program of China (2013CB956502), National Natural Science Foundation of China (41406043, 41406002), the Fundamental Research Funds for the Central Universities (15lgpy26), and the Strategic Priority Research Program of the Chinese Academy of Sciences (No. XDA11010202). Thanks to three reviewers' valuable comments in ocean science discussion. Thanks to text-check company for English revision. Prof. Bo Qiu in Hawaii University and associated Prof. Wei Zhuang in SCSIO were thanked for their valuable comments in improving this manuscript. We appreciated Remote Sensing System for their AMSR-E SST data. We also thank NCEP/NCAR products. The data in this paper will be available from the first author or corresponding author upon request after publication, and the users must promise that all data will be used only for scientific research.

References

de Boyer Montegut, C., G. Madec, A. S. Fischer, A. Lazar, and D. Iudicone (2004), Mixed layer depth over the global ocean: An examination of profile data and a profile-based climatology, *J. Geophys. Res.*, **109**, C12003, doi:10.1029/2004JC002378.

Ducet, N., P.-Y. Le Traon, and G. Reverdin (2000), Global high resolution mapping of ocean circulation from Topex/Poseidon and ERS-1 and -2. *J. Geophys. Res.*, **105,** 19477–19498.

Friehe C.A., W.J. Shaw, D.P. Rogers, K.L. Davidson, W.G. Large, S.A. Stage, G.H. Crescenti, S.J.S. Khalsa, G.K. Greenhut, F. Li(1991), Air–sea fluxes and surface layer turbulence around a sea-surface temperature front, *J. Geophys. Res.*, **96**, 8593–8609.

Gill, A. E., Atmosphere-OceanD ynamics, Academic, San Diego, Calif., 1982.

Hosoda, K. (2010), A Review of Satellite-Based Microwave Observations of Sea Surface Temperatures. *J. Oceanogr.*, **66**, 439-473.

Isoguchi, O., H. Kawamura, and T. Kono (1997), A study on wind-driven circulation in the subarctic North Pacific using TOPEX/POSEIDON altimeter data, J. Geophys. Res., 102(C6), 12,457–12,468.

Kara A.B., P.A.Rochford, and H.E. Hurlburt, 2003: Mixed layer depth variability over the global

ocean. *J. Geophys. Res.*, **108**(C3), 3079. Doi:10.1029/2000JC000736.

Kobashi F, Kawamura H (2001) Variation of sea surface height at periods of 65–220 days in the subtropical gyre of the North Pacific. J Geophys Res 106:26817–26831. doi:10.1029/2000JC000361.

Kobashi, F., S-P Xie, N. Iwasaka, and T. Sakamoto (2008), Deep atmospheric response to the North Pacific Oceanic Subtropical Front in spring. *J. Clim.*, **21,** 5960–5975.

Kobashi, F., and S-P Xie (2012), Interannual variability of the North Pacific Subtropical Countercurrent: Role of local ocean-atmosphere interaction. *J. Oceanogr.*, **68**, 113-126, doi: 10. 1007/s10872-011-0048.x.

Kobashi, F., and A. Kubokawa (2012), Review on North Pacific Subtropical Countercurrents and Subtropical mode waters in ocean circulation and climate. *J. Oceanogr.*, **68**(1), 21-43, doi: 10.1007/s10872-011-0083-7.

Levitus, S. (1982), Climatological Atlas of the World Ocean, NOAA Professional Paper 13, U.S. Department of Commerce.

Monterey, G. I., and S. Levitus (1997), Climatological cycle of mixed layer depth in the world ocean, report, 5 pp., NOAA, Silver Spring, Md.

Qiu, B. (2002), Large-scale variability in the midlatitude subtropical and subpolar North Pacific Ocean: Observations and causes, *J. Phys. Oceanogr.*,32(1), 353–375.

Qiu, B., and R. Lukas (1996), Seasonal and interannual variability of the North Equatorial Current, the Mindanao Current, and the Kuroshio along the Pacific western boundary, *J. Geophys. Res.*,101,12,31512,330, doi:10.1029/95JC03204.

Qiu, C., and H. Kawamura (2012), Study on SST front disappearance in the subtropical North Pacific using microwave SSTs. *J. Oceanogr.*, **68**, 417-426.

Qiu, C., H.Kawamura, H.Mao and J.Wu, 2014. Mechanisms of the disappearance of sea surface temperature fronts in the subtropical North Pacific Ocean. *J. Geophys. Res.*,, doi:10.1002/2014JC010142.

Sugimoto S., and K. Hanawa, 2014. Influence of Kuroshio Path Variations south of Japan on formation of subtropical mode water. *J. Phys. Oceanogr*. **44**, 1065–1077. doi: http://dx.doi.org/10.1175/JPO-D-13-0114.1

Small, R.J., S. deSzoeke, S-P Xie, L. O'Neil, H. Seo, Q. Song, P. Cornillon, M. Spall, and S. Minobe, (2008), Air-sea interaction over ocean fronts and eddies. *Dyn. Atmos. and Oceans*, **45**, 274-319.

Sun, C. & Co-Authors (2010), The Data Management System for the Global Temperature and Salinity Profile Programme, in Proceedings of OceanObs.09: Sustained Ocean Observations and Information for Society (Vol. 2), Venice, Italy, 21-25 September 2009, Hall, J., Harrison,

D.E. & Stammer, D., Eds., ESA Publication WPP-306, doi:10.5270/OceanObs09.cwp.86.

Stammer, D., 1997: Steric and wind-induced changes in TOPEX/POSEIDON large-scale sea surface topography observations.*J. Geophys. Res.*, **102,** 20 987–21 009.

Uda, M., and K. Hasunuma (1969), The eastward subtropical countercurrent in the western North Pacific Ocean. *J. Oceanogr. Soc. Jpn.*, **25**(4), 201–210.

White WB, Hasunuma K, Solomon H (1978) Large-scale seasonal and secular variability of subtropical front in the western North Pacific from 1954 to 1974. J Geophys Res 83:4531–4544.

Xie, S-P (2004), Satellite observations of cool ocean-atmosphere interaction. *Bull. Amer. Meteor Soc.*, **85,** 195-208.

Figure legends:

Figure 1. Topography of study area. The black box is the subtropical front zone defined by Qiu et al.[2014].

Figure 2. a) Zonal averaged [130 ˚E-160 ˚E] sea surface temperature gradient magnitude from January, 2003 to December, 2009; (b) monthly mean frontal position and (c) climate mean position with the standard deviations (grey shaded). Color indicates different month. Frontal position is defined as the maximum value of SST gradient magnitude.

Figure 3. Zonal mean [130-160°E] of SLA (a), steric component of SSHA calculated from (b) net heat flux, and (c) *in situ* observations.

Figure 4. Spatial structure of EOF of SLA (a) mode 1st, (b)mode 2nd, (c) mode 3rd, (d) mode 4th, and (e)time serials of EOFs. Solid line, dot line, break line, and break dot line are the first mode, second mode, third mode and fourth mode, respectively.

Figure 5. Spatial structure of EOF of SSTA (a) mode 1st, (b)mode 2nd, (c) mode 3rd, (d) mode 4th, and (e)time serials of EOFs. Solid line, dot line, break line, and break dot line are the first mode, second mode, third mode and fourth mode, respectively.

Figure 6. Scatter-plots of (a) SST and SLA, (b) SST and steric height, and (c) high-pass filtered SST and SLA in cold, front, and warm zone. Color indicates different months from April to September.

Figure 7. Temporal variations of temperature profiles in (a) cold, (b) front, and (c) warm zones. Grey double-headed arrows indicate the range of SSTs, and black double-headed arrows are the range of mixed layer depths.

Figure 8.Relationship between SST and MLD in (a) cold(back dots) and warm(grey dots) zones, (b) front zone (grey dots). Red lines is the regression line. Black line is the mean MLD every 1 ˚C, and the standard deviations are added. The red circle shows some singular points out of the envelope of standard deviations. (c) an example of the singular point position and SST distribution on April 7, 2004. The background is SST, and grey dot is the match-up position in (c).

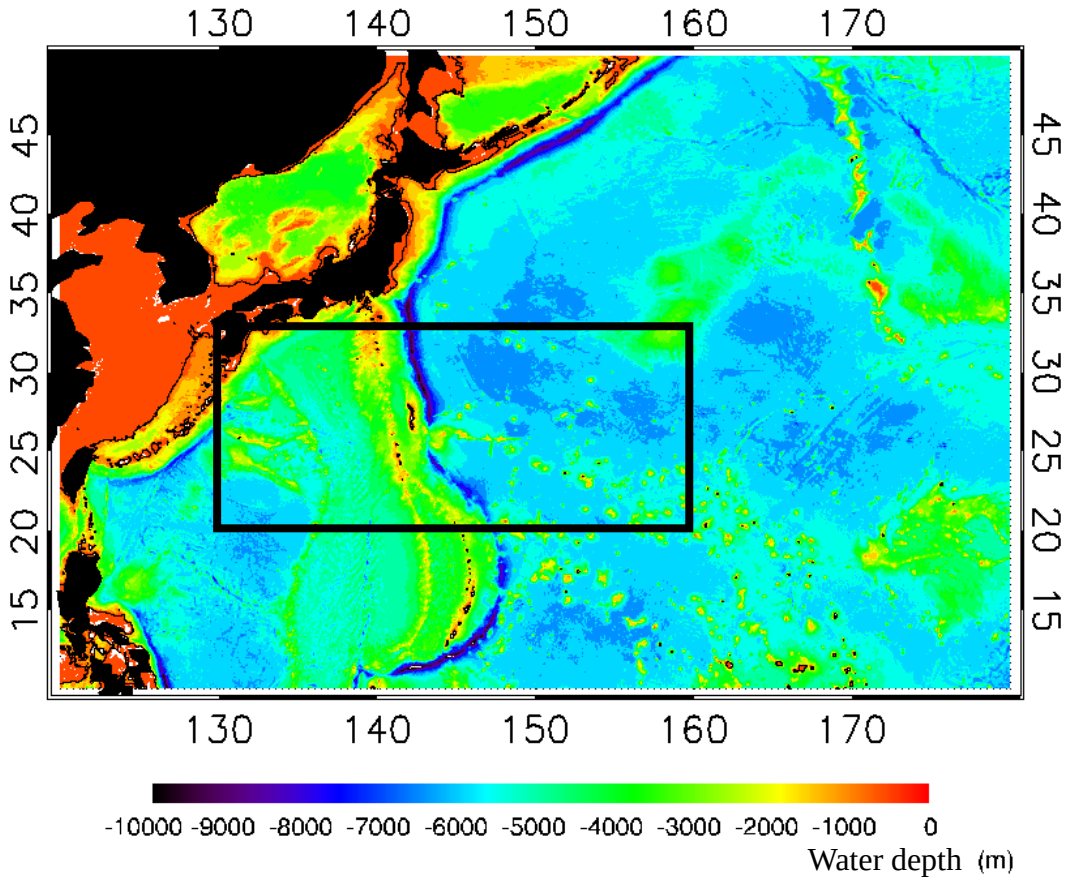

Figure 1 Qiu et al. , 2014

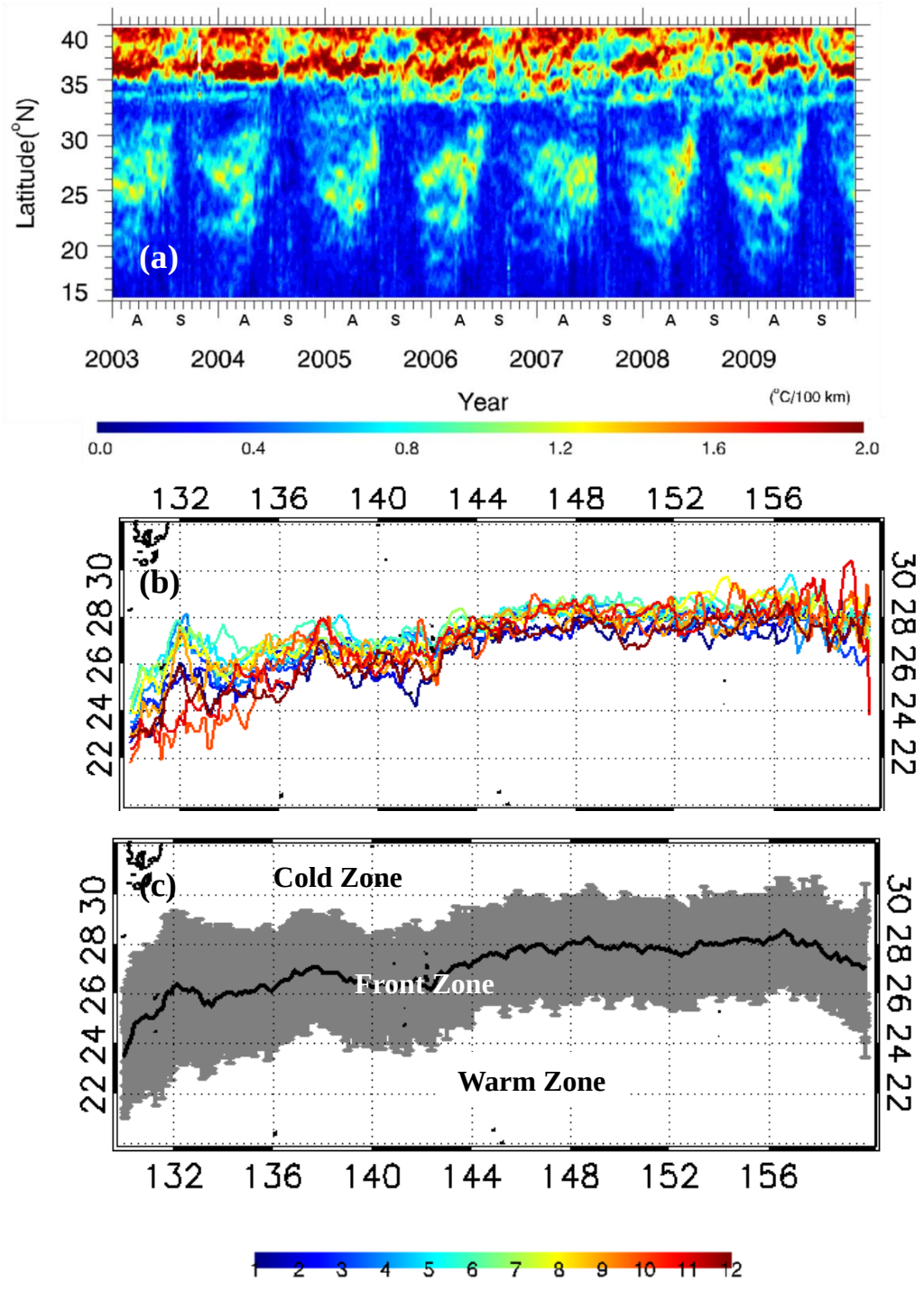

Figure 2 Qiu et al. , 2014

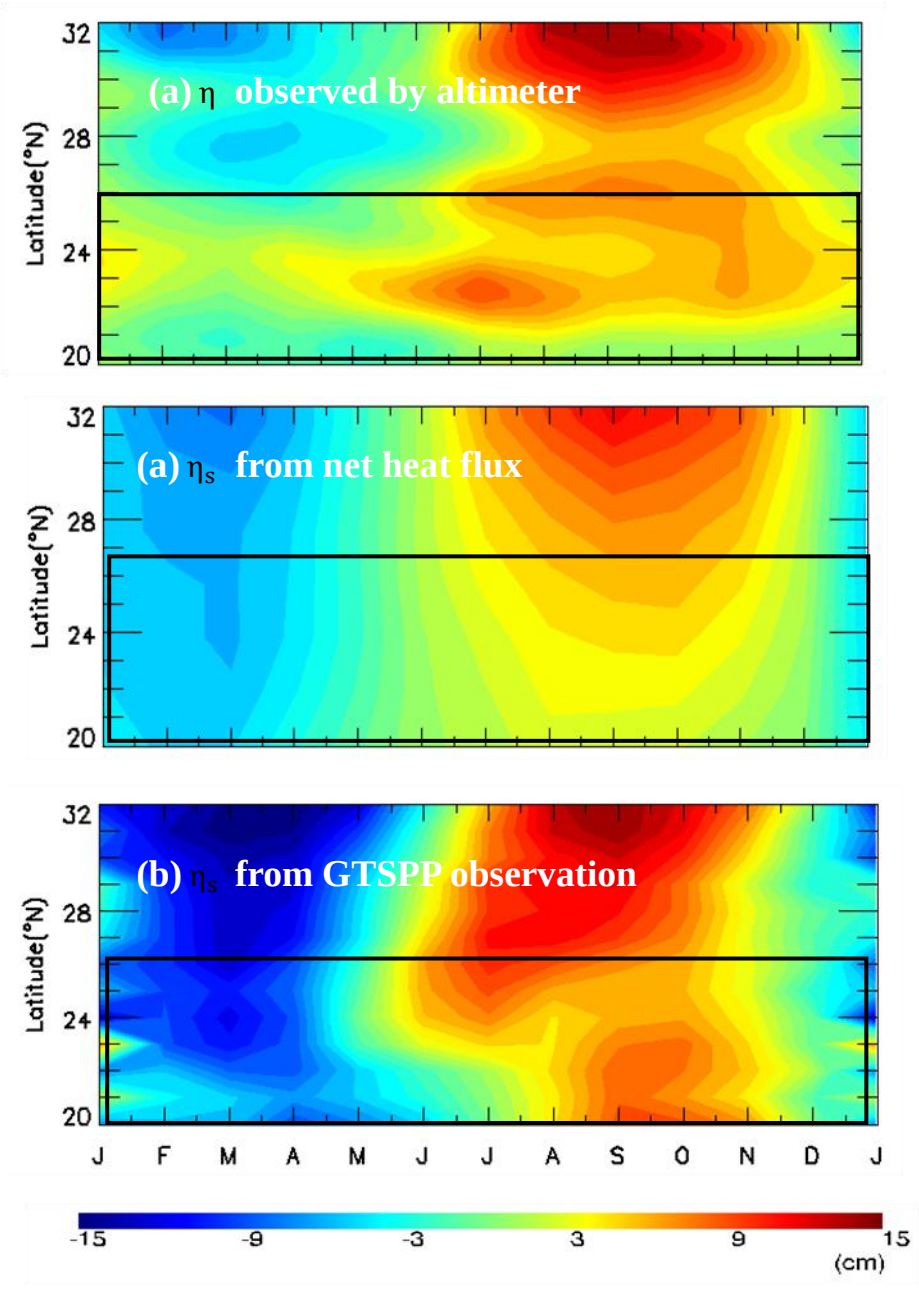

Figure 3 Qiu et al., 2014

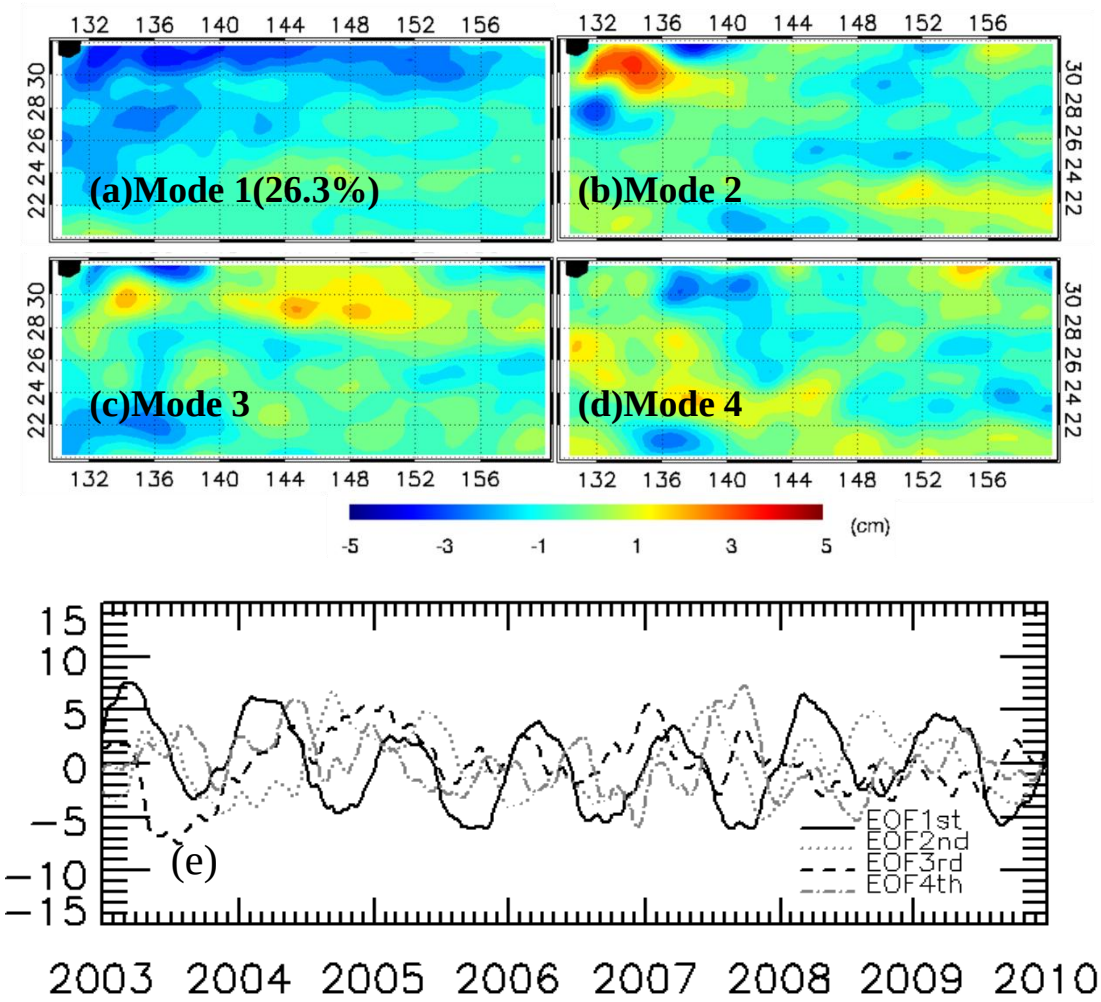

Figure 4 Qiu et al. , 2014

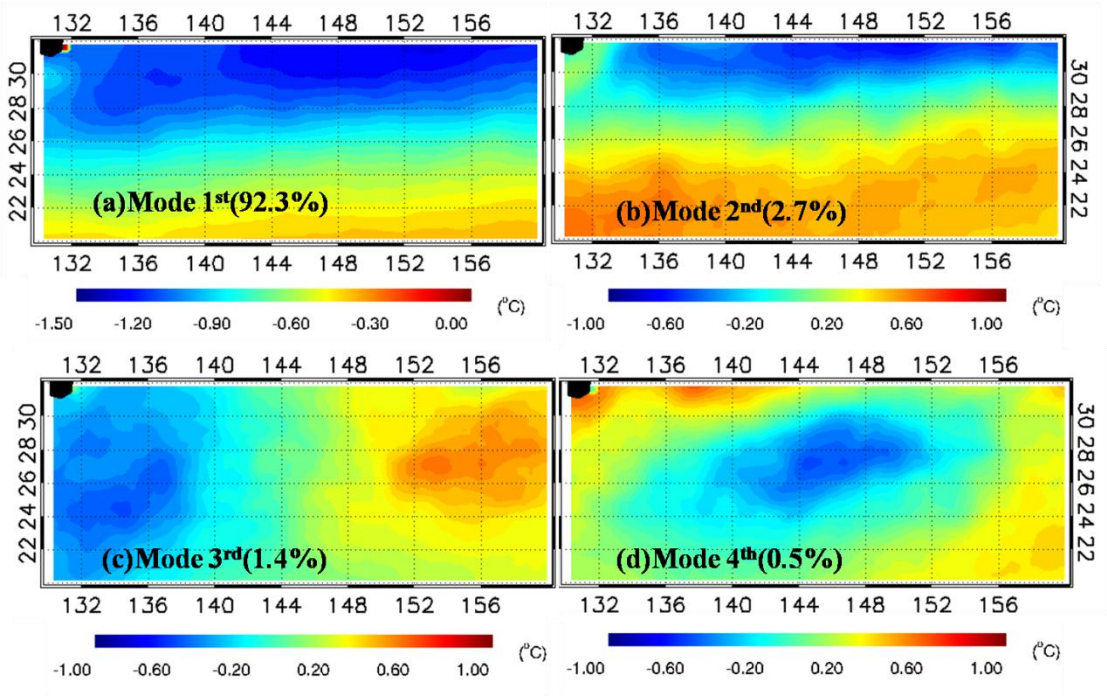

443

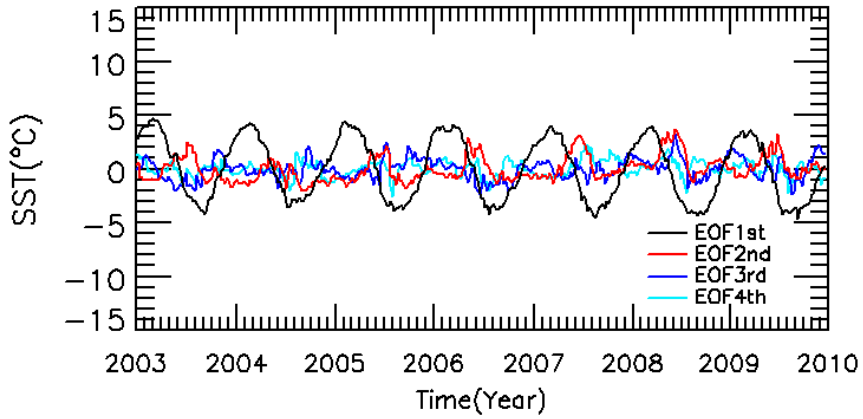

444

445 Figure 5 Qiu et al. , 2014

446

447

448

449

450

451

452

453

454

455

456

457

458

459

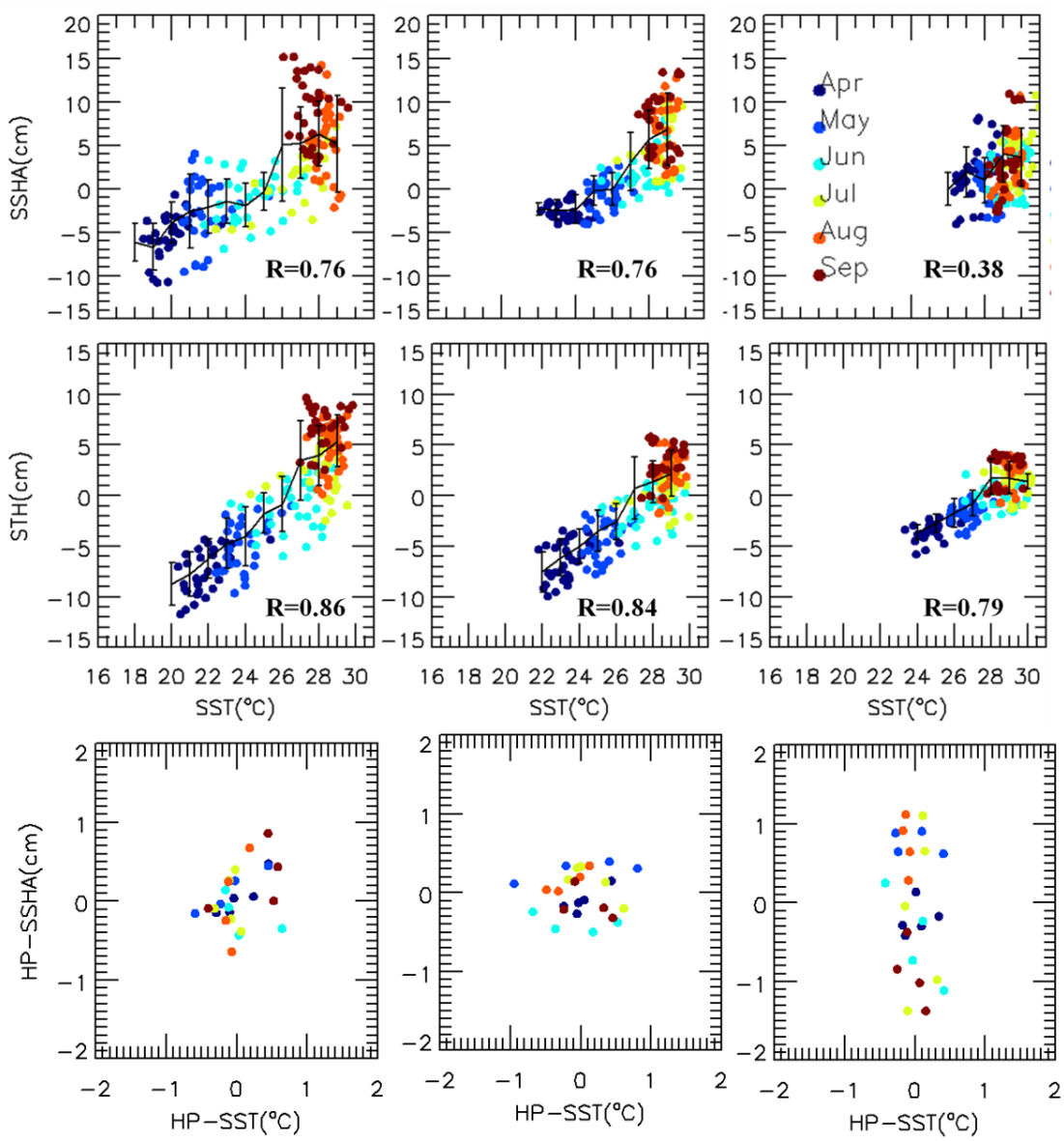

Figure 6 Qiu et al., 2014

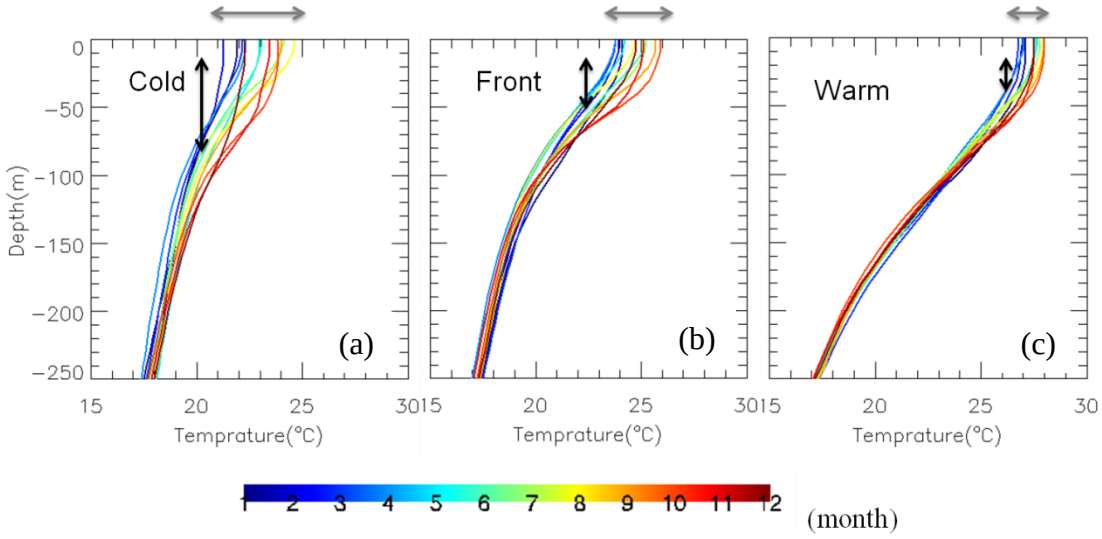

Figure 7 Qiu et al., 2014

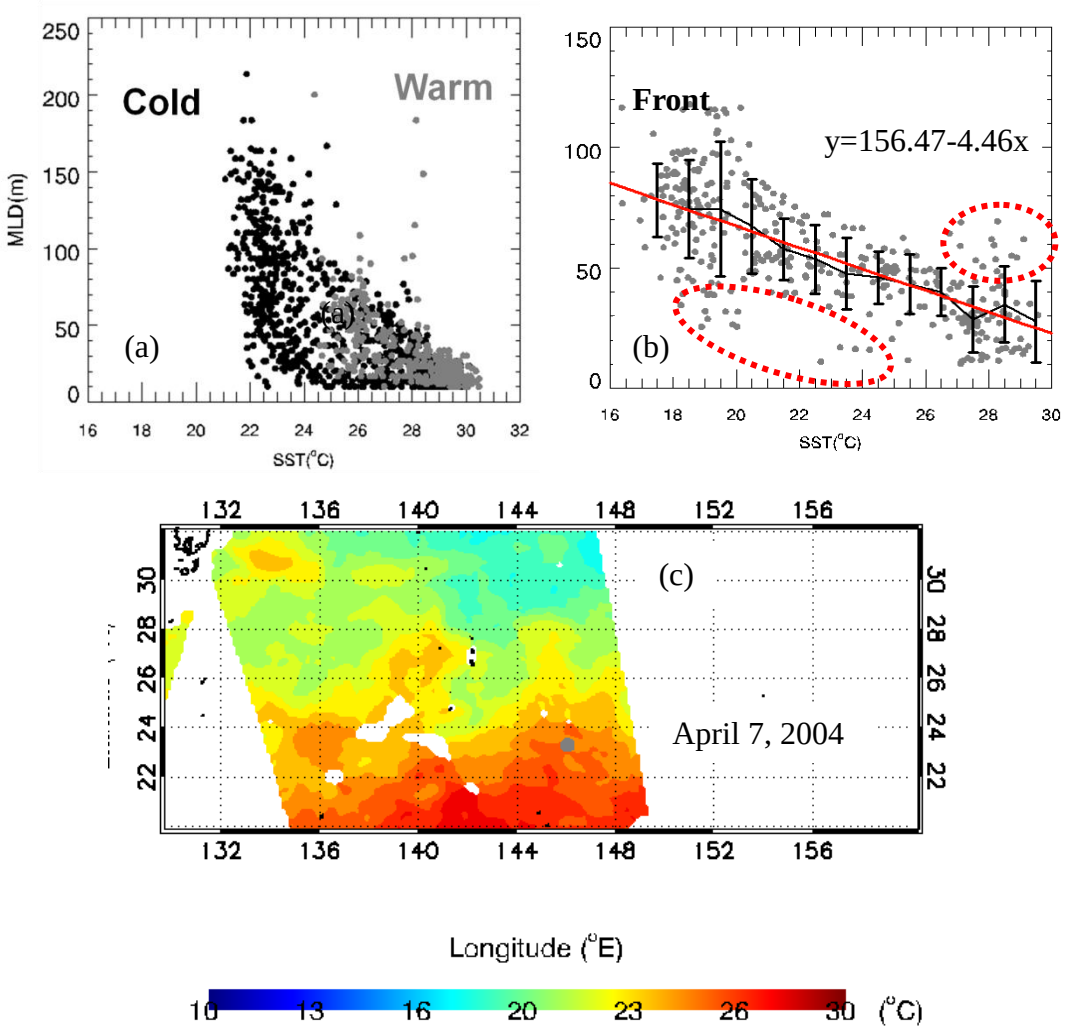

Figure 8 Qiu et al., 2014